STATISTICS OF THE SEA SURFACE DERIVED FROM SUN GLITTER[1]

By

CHARLES COX AND WALTER MUNK

Scripps Institution of Oceanography

ABSTRACT

Aerial photographs of the sun's glitter on the sea surface, taken under carefully chosen conditions in the Hawaiian area, were coordinated with measurements of winds (1–27 knots) from a vessel. Statistics of the glitter, interpreted in terms of the statistics of the slope distribution of the sea surface, gave the following results: (1) As a first approximation the slope distribution is found to be Gaussian; this can be accounted for by an arbitrarily wide *continuous* spectrum of ocean waves, but not by a spectrum consisting of a few discrete frequencies. (2) The ratio of the up/down-wind to crosswind components in mean square slope is less than two; this indicates a directional "beam width" in excess of 130° for the relatively short waves that contribute to the slope spectrum. (3) The mean square slope, regardless of direction, increases linearly with wind speed and reaches a value of $(\tan 16°)^2$ for a wind speed of 14 m sec^{-1}; this empirical relation follows in form and to an order of magnitude from a spectrum proposed by Neumann on the basis of wave amplitude observations. A spectrum proposed by Darbyshire cannot be reconciled with our observations.

Further results which have not been interpreted are: (4) An up- and down-wind skewness which increases with increasing wind speed is such as to make the most probable slope a few degrees rather than zero, with the azimuth of ascent pointing downwind. (5) A peakedness, which is barely above the limit of observational error, is such as to make the probability of very large and very small slopes greater than Gaussian. (6) Oil slicks laid by the vessel over an area of one quarter square mile reduce the mean square slope by a factor of two or three and eliminate skewness but leave peakedness unchanged.

The distribution of particle acceleration is closely related to the distribution of slope. Accordingly, the total mean square acceleration increases linearly with wind speed and reaches a value (at the surface) of $(0.4\ g)^2$ at a wind speed of 14 m sec^{-1}.

1. INTRODUCTION

If the sea surface were absolutely calm, a single mirror-like reflection of the sun would be seen at the *horizontal specular point.* In the usual case there are thousands of "dancing" highlights. At each highlight there must be a water facet, possibly quite small, which is so inclined

[1] Contribution from the Scripps Institution of Oceanography, New Series, No. 731. This work has been sponsored by the Geophysics Research Directorate of the Air Force Cambridge Research Center, under Contract No. AF 19(122)–413.

as to reflect an incoming ray from the sun toward the observer. The farther the facet is from the horizontal specular point, the larger must be its slope in order to reflect the sun's rays back to the observer. The distribution in the glitter pattern is therefore closely related to the distribution of surface slopes.

In order to exploit this relationship, plans were laid in 1951 for coordination of aerial photographs of glitter from a B-17G plane with meteorological measurements from a 58-foot schooner, the REVERIE. The first measurements were made in July 1951 offshore from Monterey, California, where a variety of wind conditions could be expected. But one of the requirements for photographing the sun's glitter is sunshine. Unfortunately the number of clear days was even fewer than those given on climatological charts, hence only two successful flights were completed. Accordingly, plane and vessel were moved to Hawaii, where one can select radically different wind conditions by moving short distances. The island of Maui was chosen because the region surrounding this island is the least clouded in the Hawaiian area. Also, the harbor and airport facilities are conveniently near to one another. Conditions were excellent, and all observations were taken during the period 25 August to 25 September 1951.

Since the air borne instrumentation has been described by Cox and Munk (1954), we shall limit ourselves to a few comments on measurements from the vessel. Bendix Friez Aerovane anemometers were installed on the fore masthead (41 ft) and bowsprit (9 ft) of the REVERIE. At the time the aerial photographs were taken, the vessel would heave to, with the wind abeam, and be steadied by sails. With this arrangement the error inherent in using cup-type anemometers on a rolling vessel can be avoided. The output of the masthead anemometer and the difference between that and the bowsprit anemometer were smoothed by an R, C-filter with 18-second time constant and were recorded on two Esterline-Angus milliammeters. Wind direction was estimated by eye. For some of the earlier measurements we attempted to raise and lower a hand anemometer with the movement of boat and waves so as to keep it 3 ft above the water surface. Other measurements included air and water temperatures, and wet and dry bulb temperatures.

One of the objects of this investigation was a study of the effect of surface slicks. Early attempts to spray powdered Atco-grain detergent from vessel or plane were unsatisfactory. In the method adopted, oil was pumped on the water, the mixture consisting of 40% used crank case oil, 40% diesel oil, and 20% fish oil. With 200 gallons of this mixture, a coherent slick 2000 by 2000 ft could be laid in 25 minutes, provided the wind did not exceed 20 mph.

2. METHOD

Here we limit ourselves to a brief review of the method, since a full discussion is given by Cox and Munk (1954). Two pairs of aerial cameras, mounted in the plane, were wired for synchronous exposure. Each pair consisted of one vertical and one tilted camera with some overlap in their fields of view. One pair gave ordinary *image* photographs for the purpose of locating cloud shadows, slicks, and vessel; this pair also gave the positions of the horizon and the plane's shadow (to correct for the roll, pitch and yaw of the plane). The other pair of cameras, with lenses removed, provided *photometric* photographs. Sample photographs are shown in Figs. 1 and 2.

The method consists essentially of two phases. The first identifies, from geometric considerations, a point on the sea surface (as it appears on the photographs) with the particular slope required at this point for the reflection of sunlight into the camera. This is done by suitable grid overlays (see Figs. 1 and 2). Lines of constant α (radial) give the azimuth of ascent to the right of the sun; lines of constant β (closed curves) give the tilt in degrees. The grids depend on the elevation ϕ of the sun and on the orientation of the camera but not on the height of the camera. The effect of the setting sun is to concentrate the pattern along a narrow street (Fig. 1).

The second phase interprets the average brightness of the sea surface (darkening on the photometric negative) at various α,β-intersections in terms of the frequency with which this particular slope occurs. At the horizontal specular point the sea surface is apt to be so bright as to be blinding to the eye, whereas at some distance from this point the surface is much darker. The principal reason for this variation is that the gentle slopes (required for highlights near the horizontal specular point) occur more frequently than steep slopes. On the *density photographs* the glitter pattern appears as a round blob with a bright core (on the positive print) and a gradually diminishing intensity to the outside (Fig. 1, lower right). The density, D, of the blob on the negative is then measured with a densitometer at points which correspond to the intersection of appropriate grid lines. Factors other than the slope probability enter into the problem and have to be allowed for.

In addition to the reflection of the sun's rays from the sea surface, there are two other distinct sources of radiation: (1) the skylight reflected at the sea surface, and (2) the sunlight scattered by particles beneath the sea surface. We have attempted to correct for these. The disappearance of the glitter into this background imposes the essential limitation on the determination of the probability of large (and infrequent) slopes.

3. RESULTS

The results of these measurements are tabulated values of slope probability for various values of α,β. Instead of presenting these tabulated values we achieve compactness by giving the results in analytical form as a function of wind speed, thus bringing out the essential physical content. In this way the experimental error is also subdued. A reasonable approach is to make use of the fact that the distribution is close to Gaussian. By representing the data as a Gram-Charlier series we can develop the deviations from the normal distribution in a systematic manner. These deviations represent skewness and peakedness and therefore have a simple physical interpretation.

Some notation has to be introduced. Let x designate the crosswind coordinate, y the upwind coordinate, and z the elevation of the surface; furthermore, let β be the tilt and $m = \tan\beta$ the slope (regardless of direction) of a small element of sea surface, and let α be its azimuth of ascent to the right of the *wind* (not of the sun, as before). Then

$$z_x = \partial z/\partial x = m \sin\alpha, \qquad z_y = \partial z/\partial y = m\cos\alpha \tag{1}$$

are the crosswind and upwind components of slope. Since the mean sea level is nearly horizontal over large distances, it follows that the mean values of z_x, z_y (averaged over many waves) are zero. However, the mean values of z_x^2, z_y^2 do not vanish and will be designated by σ_c^2, σ_u^2. Hence σ_c, σ_u are the crosswind and upwind rms slope components. The corresponding "standardized" components are defined by

$$\xi = z_x/\sigma_c, \qquad \eta = z_y/\sigma_c\,. \tag{2}$$

Now let p be the probability of slopes. More precisely, let

$$p\,dz_x\,dz_y; \qquad p\,m\,d\alpha\,dm; \qquad p\tan\beta\sec^2\beta\,d\alpha\,d\beta$$

designate the probabilities that the slopes lie within the limits

$$z_x \pm \tfrac{1}{2}dz_x,\ z_y \pm \tfrac{1}{2}dz_y; \quad \alpha \pm \tfrac{1}{2}d\alpha,\ m \pm \tfrac{1}{2}dm; \quad \alpha \pm \tfrac{1}{2}d\alpha,\ \beta \pm \tfrac{1}{2}d\beta.$$

Which of these three equivalent forms is convenient depends on the particular problem under consideration. Our measurements show that p can be adequately represented by the expression

$$\begin{aligned} p = (2\pi\sigma_c\sigma_u)^{-1}\exp\left[-\frac{1}{2}(\xi^2+\eta^2)\right]\Big\{1 &- \frac{1}{2}c_{21}(\xi^2-1) \\ &- \frac{1}{6}c_{03}(\eta^3-3\eta) + \frac{1}{24}c_{40}(\xi^4-6\xi^2+3) \\ &+ \frac{1}{4}c_{22}(\xi^2-1)(\eta^2-1) + \frac{1}{24}c_{04}(\eta^4-6\eta^2+3)\Big\} \end{aligned} \tag{3}$$

for slopes up to $\xi = \eta = 2.5$.

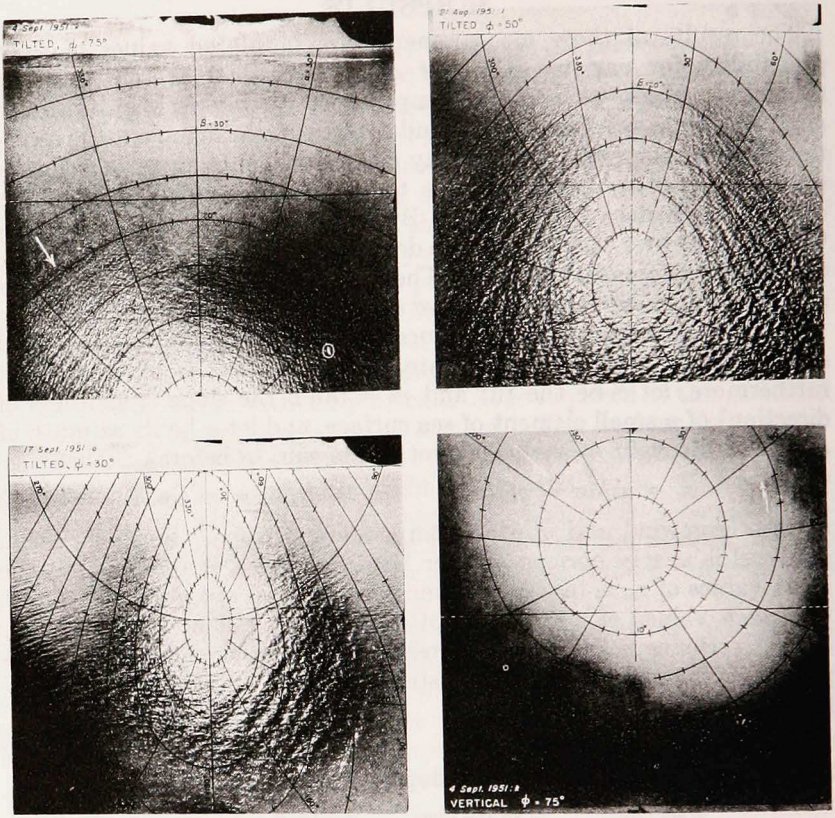

Figure 1. Upper Left and Right and Lower Left: The glitter pattern at solar elevations of ϕ = 75°, 50° and 10° respectively. The superimposed grids consist of lines of constant slope azimuth α (radial) drawn for every 30° and of constant tilt β (quasi-elliptical) for every 5°. The vessel Reverie is encircled in upper left photograph. The white arrow indicates wind direction. Lower Right: Photometric photograph. Broken arrow indicates light circle due to Reverie.

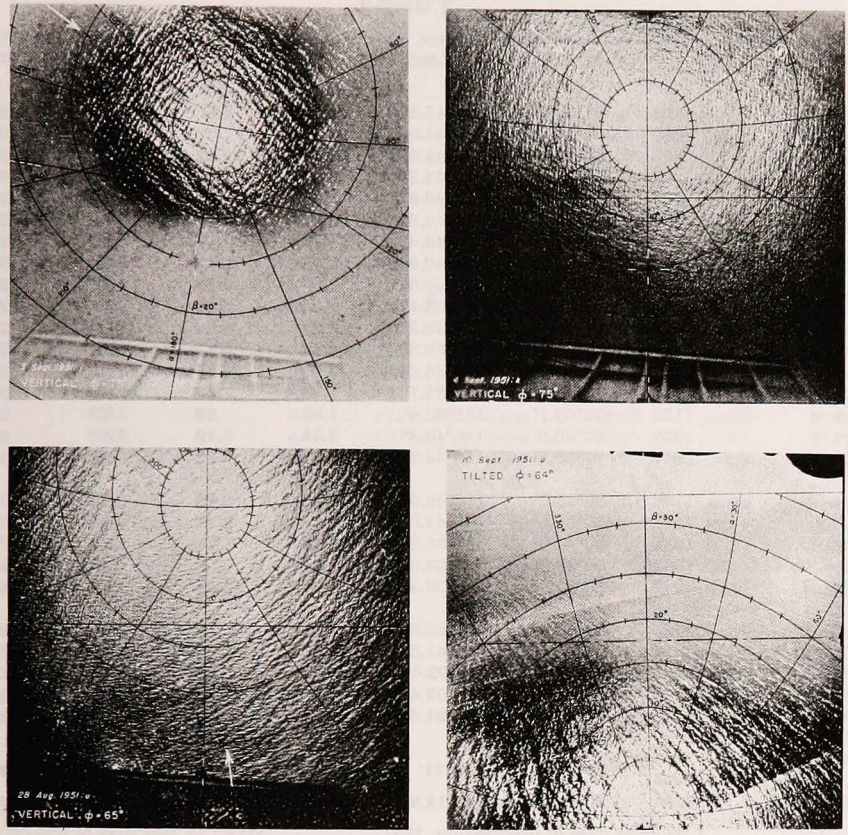

Figure 2. Upper Left and Right and Lower Left: The glitter pattern at wind speeds of 0.7, 3.9 and 14 m s^{-1} respectively. Large rotation of grid in upper left photograph is due to bad yaw as indicated by off-center position of plane's shadow (within white cross). Lower Right: A rectangular artificial slick, with near boundary almost through specular point. Brightness of slick sea surface is reduced for large β and somewhat increased for small β.

TABLE I

*Photograph Designation**	*Time†*	*Location of cameras*		*Wind*		*Direction*	*Temp. (°C) Sea Surface*
		N. Lat.	*W. Long.*	*Speed ms⁻¹*			
				41 ft#	*9 ft#*	*(true)*	
28 Aug. b	1106	21°01.8′	156°45.8′	11.6	9.6	060°	26.15°
28 Aug. p	1336	20°59.0′	156°44.0′	13.3	11.0	050°	26.4°
28 Aug. u	1403	20°58.2′	156°43.3′	13.8	11.6	050°	26.3
28 Aug. v	1403	20°58.2′	156°43.3′	13.7	11.5	050°	26.3°
3 Sept. j	1157	20°39.5′	156°46.6′	.72	.45	050°	26.51°
3 Sept. q	1330	20°39.5′	156°46.6′	8.58	7.11	120°	26.49°
3 Sept. t	1357	20°39.5′	156°46.6′	.89	.54	180°	26.51°
4 Sept. e	1126	20°40.2′	156°40.3′	1.79	.49	045°	25.90°
4 Sept. k	1158	20°39.0′	156°40.0′	3.93	3.58	100°	26.10°
4 Sept. n	1257	20°39.5′	156°36.9′	8.00	6.62	100°	26.20°
4 Sept. r	1324	20°40.0′	156°39.3′	6.30	5.27	111°	26.20°
4 Sept. v	1327	20°40.0′	156°39.3′	6.44	5.4	111°	26.20°
4 Sept. y	1353	20°39.5′	156°36.9′	4.92	4.07	110°	26.20°
5 Sept. b	1058	20°40.5′	156°35.7′	1.83	1.43	280°	26.6°
5 Sept. g	1124	20°40.1′	156°35.4′	1.39	.58	280°	26.7°
5 Sept. j	1354	20°46.8′	156°40.3′	3.35	2.99	225°	27.09°
6 Sept. c	1048	20°58.5′	156°45.3′	10.8	9.12	045°	25.95°
6 Sept. k	1124	20°58.0′	156°44.5′	10.2	8.85	045°	25.99°
6 Sept. q	1237	20°57.5′	156°44.0′	11.7	9.92	045°	26.3°
10 Sept k	1328	20°40.0′	156°38.3′	8.45	7.24	130°	26.60°
10 Sept. m	1333	20°40.0′	156°38.3′	7.15	6.00	130°	26.60°
10 Sept. r	1347	20°39.7′	156°39.3′	5.32	4.47	120°	26.59°
11 Sept. e	1317	20°45.5′	156°41.8′	5.45	3.75	210°	27.2°
11 Sept. f	1317	20°45.5′	156°41.8′	5.45	3.75	210°	27.2°
13 Sept. e	1308	20°17.6′	156°02.4′	2.41	1.97	090°	27.35°
13 Sept. f	1308	20°17.6′	156°02.4′	2.41	1.97	090°	27.35°
17 Sept. e	1136	20°29.9′	156°24.8′	9.79	8.31	086°†††	26.80°
17 Sept. c, h, k, n, q # #	{1111 / 1205}	20°28′	156°24′	9.74	8.18	088°†††	26.80°
17 Sept. A	1424	20°17.6′	156°14.8′	10.5	8.45	068°†††	26.90°

* Includes date of observation, 1951.
† Time meridian 150° W.
# Elevation above sea level.
# # Probability distribution derived from 5 photographic sets.

Values of the rms slope components σ_c, σ_u are given in Table I together with other pertinent data. The values will be different under different wind conditions, and in general they will depend on whether the sea surface is, or is not, covered by oil.

Equation (3) can be interpreted geometrically as follows. Let the two horizontal axes designate z_x, z_y and let the vertical axis designate the value of $p(z_x, z_y)$. The bell-shaped surface $p(z_x, z_y)$ is high near the coordinate center (representing the high probability of small slope) and falls off in all directions. The total volume under the curve is unity. In the case of high winds this volume is low and wide; for low winds it is high and narrow. The volume of a prism centered at z_x, z_y

TABLE I

Temp. (°C) Air at 2m	*Humidity* (%)	*Significant waves* Ht (ft)	Period (sec)	Direction (true)	*Sea Surface*	χ *+Sun Az* **	*Mean Square Slope Components* σ_c^2	σ_u^2
28.0°	69	3.5	4		clean	063°	.0211	.0390
27.75	69	6	5	056°	clean	057°	.0294	.0484
27.5°	65	6	5	056°	clean	036°	.0287	.0452
27.5°	65	6	5	056°	clean	047°	.0276	.0404
29.0°	58	1.5	3	059°	clean	095°	.00337	.00489
28.75°	61	2	3	101°	clean	140°	.0224	.0230
29.0°	58	—	—	—	clean	***	.0152	.0153
27.2°	69	1	2	120°	Nat. slick	120°	.00096	.00126
27.9°	67	1	2	100°	clean	94°	.00694	.00977
28.0°	69	2	3	106°	clean	126°	.0136	.0191
28.0°	67	4	3	106°	clean	136°	.0134	.0170
28.0°	67	4	3	106°	clean	119°	.0136	.0186
28.0°	69	4	3	100°	clean	***	.0172	.0174
27.0°	68	3	4	160°	clean	296°	.00534	.00906
27.1°	67	3	4	104°	clean	280°	.00609	.00875
27.0°	65	5	4	140°	clean	237°	.0102	.0125
27.2°	69	4	4	045°	clean	***	.0252	.0265
					oil slick	***	.0111	.0108
27.2°	71	4	4	045°	clean	040°	.0254	.0357
27.2°	69	5	4	045°	clean	045°	.0254	.0374
26.8°	81	3	3	090°	oil slick		.0102	.0117
26.8°	81	3	3	090°	oil slick	***	.00860	.0100
27.2°	76	3	3	090°	clean	***	.0137	.0179
					oil slick		.00967	.00985
27.3°	71	2	3	120°	clean	***	.0136	.0137
27.3°	71	2	3	120°	oil slick	***	.0107	.0109
28.4°	60	4	5	075°	oil slick	***	.00391	.00467
28.4°	60	4	5	075°	oil slick	076°	.00724	.00959
27.8°	76	4	3	080°	clean	080°	.0209	.0264
					oil slick		.0106	.0126
27.7°	77	4	3	080°	clean	087°	.0230	.0322
27.8°	79	5	3	080°	clean	069°	.0224	.0365

** True Azimuth of principal (y') axis.

*** Observed wind direction used.

††† Wind direction estimated from direction of wind streaks on water; recorded wind direction appears to be in error by twice magnetic variation.

with a base area $\delta z_x \delta z_y$ is the probability $p(z_x,z_y)\,\delta z_x \delta z_y$ for the occurrence of slopes within $z_x \pm \frac{1}{2}\delta z_x$, $z_y \pm \frac{1}{2}\delta z_y$.

Now take sections along various directions through the coordinate center. Each of these is nearly Gaussian and can be closely fitted by a Gaussian curve of equal standard deviation. Two of these sections (the principal sections) are of particular interest (Fig. 3): for one the equivalent Gaussian curve has greater standard deviation than any other section; the reverse is true for the other. These correspond to the direction of the smallest and largest mean square slope. Our observations show that they are oriented crosswind and up/downwind.

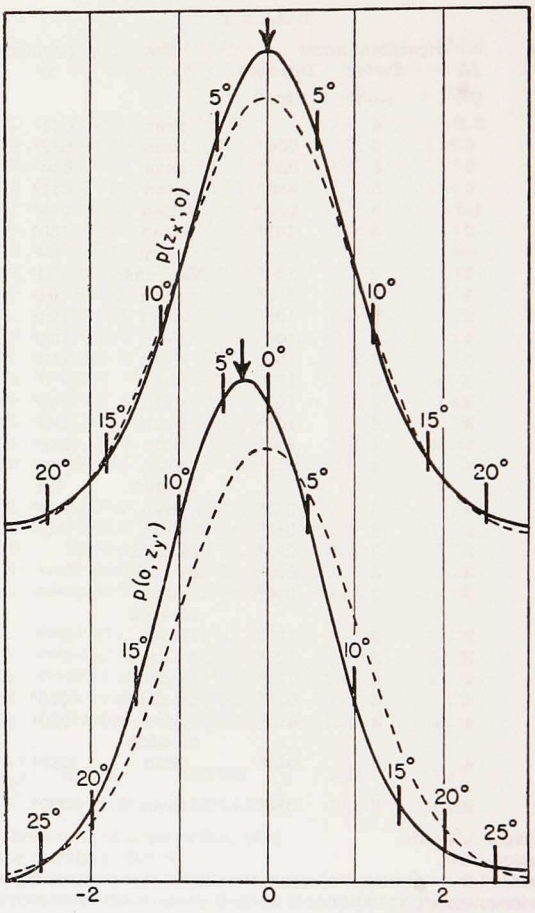

Figure 3. Principal sections through the probability distribution surface $p(z_x,z_y)$. The upper curves are along the crosswind axis z_x, the lower ones along the up/downwind axis z_y (positive upwind). The solid curves refer to the observed distribution, the dashed to a Gaussian distribution of equal mean square slope components. The thin vertical lines show the scale for both standardized slope components $\xi = z_x/\sigma_c$ and $\eta = z_y/\sigma_u$. The two scales for tilt, β, refer to a wind speed of 10 m sec^{-1}; skewness shown in the lower curve is computed for this wind speed. The modes are marked by arrows.

Another observed feature illustrated in Fig. 3 is an up- and downwind skewness. As a result, the most probable tilt is a few degrees, not zero, with the azimuth of ascent pointing downwind. Conversely, large slopes are more probable with azimuth of ascent pointed upwind. The skewness, as contained in the coefficients c_{21}, c_{03}, increases with increasing wind speed from nearly zero at very low winds to

$$c_{21} = -.11 \pm .03, \qquad c_{03} = -.42 \pm .12$$

at 14 m sec^{-1}.

The peakedness coefficients c_{40}, c_{22}, c_{04} are such as to make the very large and very small slopes more probable than those required for a Gaussian distribution (Fig. 3). The peakedness may be the result of variability in wind speed, but it is possible that systematic errors in the correction for background light may account for much of the observed peakedness. The peakedness coefficients show no significant variation with wind speed. The mean values are $c_{40} = .4 \pm .2$, $c_{22} = .1 \pm .05$, $c_{04} = .2 \pm .4$.

Oil slicks which cover an area of roughly one-fourth square mile reduce the mean square slope (regardless of direction) by a factor of two or three and eliminate skewness but leave peakedness unchanged.

There have been two other investigations of surface slopes. Duntley (1950) measured the surface slope components on Lake Winnipesaukee, N. H., by recording electrically the difference in immersion of pairs of thin vertical wires passing through the water surface. The wires were oriented to give simultaneous measurements of up/downwind and crosswind components. The separation between the wires on different occasions was 25 mm and 9 mm; consequently the measurements refer to the average value of slope over these distances. Schooley's (1954) observations from a bridge over the Anacostia River consisted of measuring the highlighted area on *resolved* photographs of the reflection of an artificial light source over the river. The results of their investigations agree in some points with ours, but there are significant discrepancies. Schooley's values of the mean square slopes are significantly *smaller* than ours for both high and low winds but agree at moderate wind speeds, whereas Duntley's values are 2.5 times *larger*. A discussion of these results has been given by Cox and Munk (1953).

4. SOME USEFUL RELATIONSHIPS

Of the many possible ways of describing the complexity of the sea surface, three in particular have been useful in modern work. Let f be some pertinent parameter with zero mean value such as elevation, slope, curvature, etc., and let $<f^2>$ be the mean square value (or variance) of f. According to the first approach, we let $\mathbf{T}_\omega \delta\omega$ be the contribution to $<f^2>$ by waves in the narrow, but not infinitely narrow (see Section 4.1), frequency band $\omega \pm \frac{1}{2}\delta\omega$. We can measure this quantity by recording it through an appropriate band pass filter, squaring the output, and averaging. It follows that

$$<f^2> = \int_0^\infty \mathbf{T}_\omega d\omega \tag{4}$$

is the mean square slope due to all frequencies. Here $\mathbf{T}_\omega$ is called the "frequency spectrum of the variance of f," or simply the spectrum.[2]

The second approach is the one we have taken. Let $p(f)df$ be the probability of slopes in the range $f \pm \frac{1}{2}df$. Then by definition

$$<f^2> = \int_0^\infty f^2 p(f) df. \tag{5}$$

Finally, a useful concept is the correlation (or mean displaced product)

$$\psi(a,b,\tau) = <f(x,y,t)f(x + a, y + b, t + \tau)> \tag{6}$$

between the value of f at position x,y and time t, and at $x + a$, $y + b$, and $t + \tau$. It is presumed that the surface is statistically uniform over time and space and that the corresponding averages are equal. For the special case $a = b = 0$, it can be shown (for example, see Rice, 1944: section 2) that the "auto correlation" is related to $\mathbf{T}$ according to

$$\psi(0,0,\tau) = \int_0^\infty \mathbf{T}_\omega \cos(\omega\tau) d\omega. \tag{7}$$

The foregoing equations show that the spectrum, the probability distribution, and the correlation are not unrelated. Our measurements of the probability distribution, therefore, have some bearing on the spectral representation of ocean waves. The required relationships, to be discussed (and made plausible, we hope) in this section, will be applied in the next.

[2] For the special case where f denotes the elevation z above mean sea level, the terms "energy spectrum" and "power spectrum" have been used. Strictly speaking, the energy spectrum is $\rho g \mathbf{T}_\omega$, as $\rho g \mathbf{T}_\omega(\omega)\delta\omega$ is the energy contained in the band $\omega \pm \frac{1}{2}\delta\omega$. The term power spectrum was originally introduced in electrical problems where it is convenient to measure the energy spectrum by recording the power dissipated in a unit resistance. But it is not suitable to oceanographic problems. An appropriate definition would be $\rho g \mathbf{v}\mathbf{S}$, where $\mathbf{v}(\omega)$ is the group velocity vector and $\mathbf{S}$ the directional spectrum of z^2 (Section 4.2). Then $\rho g \mathbf{v}\mathbf{S}(\omega, \alpha)\delta\omega\delta\alpha$ is the flux of energy in the frequency band $\omega \pm \frac{1}{2}\delta\omega$ into the direction $\alpha \pm \frac{1}{2}\delta\alpha$. This important spectrum, after integration over all frequencies, gives the angular distribution around a cylindrical island of the dissipation of energy. In deep water the magnitude of $\mathbf{v}$ is proportional to wave period, and the true power spectrum is therefore weighted in favor of the low frequencies relative to the energy spectrum.

4.1 *The frequency spectrum of the variance of elevations.* Most observations of ocean waves have been made at a single point in space, say the point $x = y = 0$. The result has been a record of $z(0,t)$ for a limited time, $2T$. Such a record may be represented in two ways. Since we have no information concerning the sea surface before or after the record, we may assume (A) that it repeats itself indefinitely over successive intervals, $2T$, or (B) that it is zero before and after the record. These assumptions lead to (A) Fourier series with periods $(2T)$, $\frac{1}{2}(2T)$, $\frac{1}{3}(2T)$, $\cdots$, or (B) Fourier integrals with all possible periods. It can be shown that the two representations are exactly the same for those periods contained in the series. For our purpose it is more convenient to use the second approach. Hence

$$z(0,t) = \int_{-\infty}^{\infty} g(\omega)e^{i\omega t}d\omega, \tag{8}$$

where

$$g(\omega) = (2\pi)^{-1}\int_{-T}^{T} z(0,t)e^{-i\omega t}dt \tag{9}$$

is the (complex) amplitude of a wave train of frequency ω.

But $g(\omega)$ is not a convenient function. It is sensitive to phase and its absolute value tends to increase as the length of record $2T$ increases. On the other hand, $|g(\omega)|^2 = g(\omega)g^*(\omega)$ is not phase-sensitive. Furthermore, it is readily measured by passing the wave-generated signal through a narrow tuned filter. Since by hypothesis the sea surface is statistically uniform in time, the mean square of the sea surface elevation must exist. According to Parseval's theorem (Titchmarsh, 1937)

$$\langle z^2(0,t)\rangle = \lim_{T\to\infty}\frac{1}{2T}\int_{-T}^{T} z^2(0,t)dt$$

$$= \lim_{T\to\infty} 2\pi\int_{-\infty}^{\infty}\frac{g(\omega)g(-\omega)}{2T}d\omega = \lim_{T\to\infty} 4\pi\int_{0}^{\infty}\frac{|g|^2}{2T}d\omega. \tag{10}$$

The last equality follows because z is a real quantity, hence from (9) $g(-\omega) = g^*(\omega)$.

The existence of the limit of the integral in (10) does not necessarily imply the existence of the limit of the integrand. It is tempting to assume that it does, for then the limit of $4\pi|g|^2/2T$ as $T \to \infty$ equals the spectrum $\mathbf{T}_\omega$ in accordance with (4). Surprisingly, this is not the case for waves which result from a large number of impulses randomly

applied to the sea surface. A plot of $|\bar{g}|^2/2T$ against ω is then a wiggly line which oscillates more and more wildly as the record length is increased. The difficulty can be removed by defining $\bar{g}^2$ as a smoothed version of $|g|^2$ averaged over an arbitrarily small but *finite* range. The limit

$$\mathbf{T}_\omega = \lim_{T\to\infty} \frac{4\pi\bar{g}^2}{2T} \tag{11}$$

then exists, and equation (10) can be written

$$<z^2> = \int_0^\infty \mathbf{T}_\omega d\omega. \tag{12}$$

A rigorous mathematical approach[3] uses a Lebesgue integral formula in place of (10).

4.2 *The directional spectrum of the variance of elevation.* In contrast to measurements at a fixed point, the slope distribution was measured at a single instant. We may connect these two types of measurements by means of the wave equation. Suppose that z and $\partial z/\partial t$ are specified at $t = 0$ within the area $-S < x < S$, $-S < y < S$. Then

$$z(x,y,t) = \mathrm{Re} \int_{-\infty}^{\infty}\int_{-\infty}^{\infty} A(k_x,k_y) \exp i(k_x x + k_y y - \omega t) dk_x dk_y \tag{13}$$

satisfies the specified initial conditions, provided (Longuet-Higgins, 1950)

$$A(k_x,k_y) = \frac{1}{2\pi}\int_{-S}^{S}\int_{-S}^{S}\left(z - \frac{1}{i}\frac{\partial z}{\partial t}\right)_{t=0} \exp - i(k_x x + k_y y) dx dy. \tag{14}$$

Equation (13) represents z as a series of elementary wave trains of wave length $2\pi/k$, where $k^2 = k_x^2 + k_y^2$, frequency $\omega(k)$, phase velocity $C = \omega/k$ in the direction of the vector (k_x,k_y), and amplitude $A(k_x,k_y)$ $dk_x dk_y$. Each elementary train obeys the wave equation $\nabla^2 z = C^{-2}\partial^2 z/\partial t^2$. The sea surface has been assumed flat at $t = 0$ for $|x| > S$, $|y| > S$, and because of this assumption the forecasting value of (13) will deteriorate with time. This difficulty can be avoided by increasing the area $4S^2$ without limit. In particular, it can be shown (Cox and Munk, 1953) that if

$$\mathbf{S} = \lim_{S\to\infty} \frac{2\pi^2\bar{A}^2}{4S^2}, \tag{15}$$

[3] See, for example, Wiener (1933). The application of the Lebesgue integral to ocean wave analysis is largely due to Pierson and his collaborators (Pierson and Marks, 1952).

where $\overline{A}^2$ is a smoothed version of $|A|^2$ (analogous to the relation between $\bar{g}^2$ and $|g|^2$), then

$$\psi(a,b,\tau) = \int_{-\infty}^{\infty}\int_{-\infty}^{\infty} S \cos(k_x x + k_y y - \omega\tau) dk_x dk_y. \qquad (16)$$

The way is now open to find the connection between the frequency spectrum, $\mathbf{T}_\omega$, and the directional spectrum $\mathbf{S}$. Setting $a = b = 0$ and changing variables from (k_x,k_y) to (ω,α), we have

$$\psi(0,0,\tau) = \int_{0}^{\infty}\int_{-\pi}^{\pi} \mathbf{S}(\omega,\alpha) \left| \frac{\partial(k_x,k_y)}{\partial(\omega,\alpha)} \right| \cos(\omega\tau) d\alpha d\omega, \qquad (17)$$

where $\partial(k_x,k_y)\partial(\omega,\alpha)$ is the Jacobian of the transformation. A comparison with (7) leads to

$$\mathbf{T}_\omega = \int_{-\pi}^{\pi} \mathbf{S}(\omega,\alpha) \left| \frac{\partial(k_x,k_y)}{\partial(\omega,\alpha)} \right| d\alpha, \qquad (18)$$

which is the desired relation.

There are two approximations inherent in the stated form of the wave equation which limit the applicability of these results: (A) nonlinear terms have been neglected and (B) no allowance has been made for generation and decay of waves. The first error may be associated with the fact that the observed distribution of slopes showed a slight positive peakedness relative to a Gaussian distribution while the linear equation predicts a strictly Gaussian distribution for the statistically steady state. The second error will cause the predicted form of the sea surface to disagree with equation (13) for $t > 0$, but if the fetch and duration of the wind are large enough so that "equilibrium waves" are present, then the statistical behavior of the sea surface is sufficiently well represented. Since very short waves generate and decay most rapidly, the uncertainty of the results is greatest for large values of k and ω.

Note that the evaluation of the directional spectrum requires a knowledge of both z and $\partial z/\partial t$ at the initial time. Clearly the information $z(x,y,0)$ from a single snapshot could not tell us whether the waves are travelling in one direction or in the opposite one. Yet the topography shown on such a snapshot can be represented by a Fourier spectrum. We shall call this the *two-dimensional* spectrum. It differs from the *directional* spectrum inasmuch as it contains only directions in the range $-\frac{1}{2}\pi$ to $+\frac{1}{2}\pi$ as compared to $-\pi$ to $+\pi$. For any particular direction, α, the two-dimensional spectrum equals $\mathbf{S}(\alpha) + \mathbf{S}(\alpha + \pi)$. If the directional spectrum is narrow and contains only small contributions from directions outside $-\frac{1}{2}\pi < \alpha < +\frac{1}{2}\pi$,

then the two spectra are nearly the same with regard to the surface elevation. However, the slight difference may be of importance at great depths where wave trains travelling oppositely lead to oscillations which Longuet-Higgins (1950) suggests are a cause of microseisms.

4.3 *Slope spectra and mean square slopes.* The relation (16) between the correlation and the directional spectrum permits a comparison of spatial observations (such as the slope distribution as determined by glitter observations) with records obtained at a single point. The starting point is equation (6), with f designating the elevation z. The method is to differentiate (6) and (16) with respect to a,b to obtain [4]

$$-\frac{\partial^2\psi}{\partial a^2} = \langle z_x(x,y,t)z_x(x+a, y+b, t+\tau)\rangle$$

$$= \int_{-\infty}^{\infty}\int k_x^2\mathbf{S}\cos(k_x x + k_y y - \omega\tau)dk_x dk_y \qquad (19)$$

$$-\frac{\partial^2\psi}{\partial b^2} = \langle z_y(x,y,t)z_y(x+a, y+b, t+\tau)\rangle$$

$$= \int_{-\infty}^{\infty}\int k_y^2\mathbf{S}\cos(k_x x + k_y y - \omega\tau)dk_x dk_y.$$

Comparison with (16) shows that $k_x^2\mathbf{S}$ and $k_y^2\mathbf{S}$ are the spectra of the slope components, z_x and z_y. For the case $a = b = 0$, equation (18) reduces to

$$\langle z_x^2\rangle = \int_{-\infty}^{\infty}\int k_x^2\mathbf{S}dk_x dk_y, \qquad \langle z_y^2\rangle = \int_{-\infty}^{\infty}\int k_y^2\mathbf{S}dk_x dk_y. \qquad (20)$$

With the y-axis pointing upwind, these are the crosswind and up/downwind components of mean square slopes σ_c^2 and σ_u^2. On changing to the variables (k,α), one obtains finally

$$\sigma_c^2 = \int_0^{\infty}\int_{-\pi}^{\pi} k^2\sin^2\alpha\mathbf{S}kdkd\alpha, \qquad \sigma_u^2 = \int_0^{\infty}\int_{-\pi}^{\pi} k^2\cos^2\alpha\mathbf{S}kdkd\alpha \qquad (21)$$

and

$$\sigma^2 = \sigma_c^2 + \sigma_u^2 = \int_{-\infty}^{\infty}\int k^2\mathbf{S}dk_x dk_y = \int_0^{\infty} k^2\mathbf{T}_\omega d\omega. \qquad (22)$$

The last expression follows from (17) and (18).

[4] For example, see Eckart (1953): eq (37).

5. INTERPRETATION

The spectrum of the sea surface has been written in different ways by different authors. We now consider whether their mathematical models are consistent with our observations. First we seek to find the simplest model consistent with two observed features: the nearly Gaussian distribution of slopes (Section 5.1) and the appropriate ratio of up/downwind to crosswind mean square slope components (5.2). These features do not place any severe restrictions on the dependence of the slope spectrum on wave frequency. In Sections 5.3 and 5.4 the more complicated models proposed respectively by Darbyshire and Neumann are examined. Only the Neumann wave spectrum is consistent with the remaining principal features of the observed slope distribution: the linear increase of mean square slope with wind speed.

5.1 *Waves in one dimension.* The simplest model consists of a set of sinusoidal waves having one frequency and one direction. If such waves existed on the ocean surface they would have infinitely long crests. The slope distribution would be one-directional and the glitter pattern would consist of a single streak along some line α = constant. Clearly this is not in accord with the pattern shown on Figs. 1 and 2.

In addition to this discrepancy, the model leads also to frequency distributions of slopes which differ essentially from the observed distribution. The most probable slopes of a single sine wave are the slopes at the inflection points (say $\pm A$), where their values are stationary—and at a maximum. The probability $p(z_x)\delta z_x$ for slopes between $z_x \pm \frac{1}{2}\delta z_x$ is given by

$$\pi^{-1}(A^2 - z_x^2)^{-\frac{1}{2}} \tag{23}$$

for $z_x^2 < A^2$, and zero otherwise. The distribution is bimodal as shown in Fig. 4.

Next we consider the linear superposition of N sine waves

$$z_x = \sum_{j=1}^{N} A_j \cos(k_j x + \varphi_j). \tag{24}$$

We assume that the ratio of any two wave numbers, k_l/k_m, is irrational. The slope component is then an example of the "almost periodic function" of H. Bohr. As implied by its name, the almost periodic function comes close to being periodic but never quite repeats itself, a property which is in accord with our impressions of the real sea surface. The irrationality of the wave number forbids that equation (24) could represent any wave phenomenon in which the waves have rational "overtones," for example, Stokes waves of finite amplitude or seiches of a shallow rectangular body of water. In the open sea these are not believed to be serious limitations.

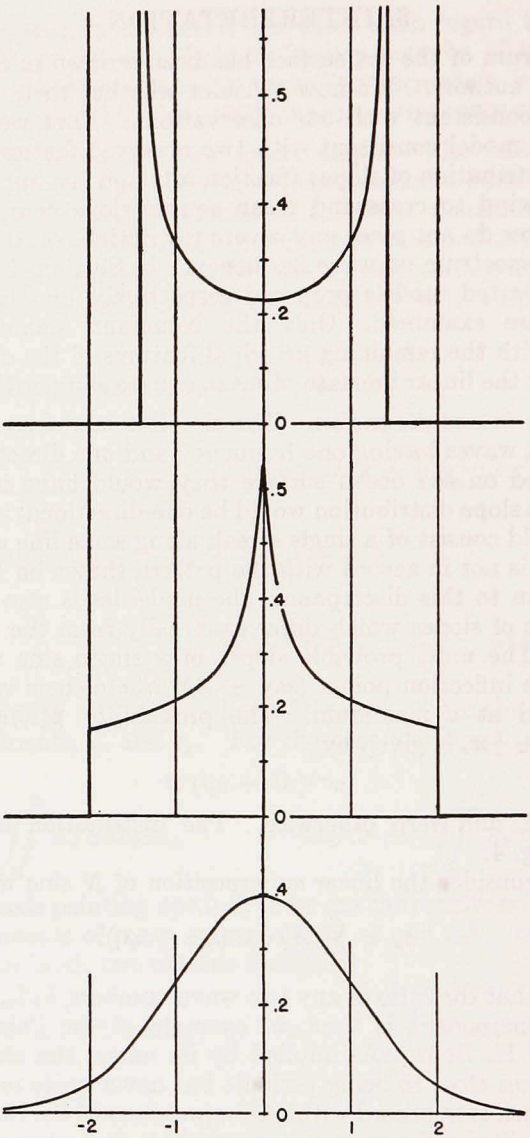

Figure 4. Top. Slope probabilities resulting from one sine wave. Middle. The linear superposition of two sine waves of equal maximum slope and irrational periods. Bottom. The linear superposition of an infinite number of irrational sine waves. The horizontal scale is $\xi = z_x/\sigma_x$; the vertical scale gives $p(z_x)$ in units of $1/\sigma_x$.

With the proviso of irrational wave numbers, the slope z_x due to any of the N components is uncorrelated with that of any other, and the calculation of the distribution of z_x is an example of the problem of random flights (for example, see Chandrasekhar, 1943). Cox and Munk (1953) found that

$$p(z_x) = \pi^{-1} \int_0^\infty \cos(\rho z_x) \left[\prod_{j=1}^{N} J_0(\rho A_j) \right] d\rho. \tag{25}$$

For the special case of a single wave number ($N = 1$), this reduces to (23); for *two* waves of equal amplitude A, this reduces to

$$\pi^{-2} A^{-1} K[1 - (z_x/2A)^2]^{-\frac{1}{2}} \tag{26}$$

for $z_x^2 < 4A^2$, and zero otherwise, where $K(x) = \int_0^{\frac{1}{2}\pi} (1 - x^2 \sin^2 t)^{-\frac{1}{2}} dt$ is the elliptic integral. In this case the distribution has a single logarithmically infinite maximum (Fig. 4). In the case of two unequal waves there would be two such maxima. For three sine waves there are no infinite peaks in the distribution function. In a general way it can be seen that the distribution approaches the Gaussian distribution as N increases. When N is large and when all N components are equal, equation (25) reduces to

$$(2\pi)^{-\frac{1}{2}} \sigma_x^{-1} e^{-\frac{1}{2}\xi^2} [1 - (\xi^4 - 6\xi^2 + 3)/(16N) + \cdots], \tag{27}$$

where σ_x^2 is the mean square slope and $\xi = z_x/\sigma_x$. This series is of the Gram-Charlier type, with the second term in the square bracket representing peakedness.[5] Comparison with equation (3) for the two-dimensional type reveals that the peakedness coefficient c_{40} is equivalent to $-(3/2N)$. Thus the foregoing expression leads to a negative peakedness, whereas the observed peakedness is positive. Hence the experimental results provide no evidence for discrete spectral components in the ocean waves.

A sea surface with a *continuous* spectrum of waves may be considered as the result of increasing the number N of discrete components without limit. In this case equation (27) reduces to a Gaussian distribution.

5.2 *"Beam width" of the trade wind sea.* In the preceding section we have learned that the observed distribution is consistent with a continuous spectrum in two dimensions. The next problem is to interpret the observed ratio σ_c^2/σ_u^2 in terms of the dependence of the directional spectrum **S** on the direction α. Clearly, if **S** were the same in all directions, then the crosswind and up/downwind slopes would

[5] A similar development can be found in Sȳno (1953).

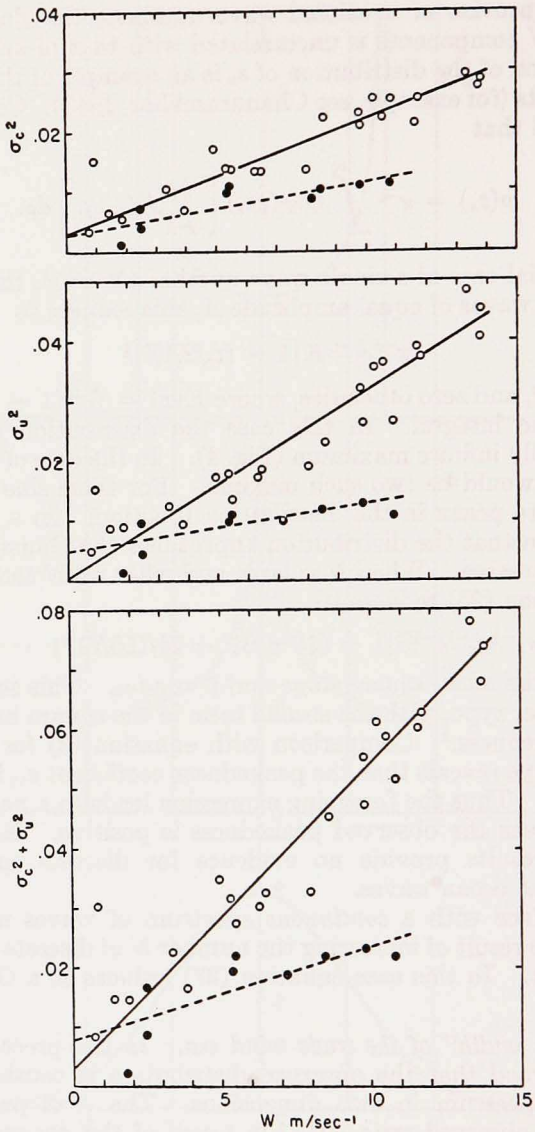

Figure 5. Mean square slope components and their sum as functions of the wind speed, W, measured 41 feet above sea level. The plot includes all analyzed data for clean sea surface (open circles) and slick surfaces (solid circles). Continuous lines are regression lines for clean surface; dashed lines for slick surface.

be equal and their ratio would be unity. On the other hand, if **S** were confined to a narrow range on both sides of the wind, then the cross-wind component would be very small compared to the up/downwind component of mean square slopes. The measured values (Fig. 5, Table I) lie between these extremes and indicate a broad but nonetheless directional "beam pattern." The large variability in the ratio σ_c^2/σ_u^2 (Table II) is far in excess of experimental error. It is probably the result of differences, from one case to the next, in the variability of the wind direction. Steady winds would lead to small values in σ_c^2/σ_u^2, whereas gusty winds would diminish this ratio to somewhere near unity.

According to equation (21),

$$\frac{\sigma_c^2}{\sigma_u^2} = \frac{\int_0^\infty \int_{-\pi}^{\pi} k^2 \sin^2 \alpha \, \mathbf{S}(k,\alpha) k dk d\alpha}{\int_0^\infty \int_{-\pi}^{\pi} k^2 \cos^2 \alpha \, \mathbf{S}(k,\alpha) k dk d\alpha}.$$

The simplest assumption we can make is that the directionality is the same for all wave numbers, k, and that the beam pattern is sharply bounded at $\alpha = \alpha_0$. Hence

$$\mathbf{S} = F(k) \quad \text{for} \quad -\alpha_0 < \alpha < \alpha_0,$$

and zero otherwise. This gives

$$\frac{\sigma_c^2}{\sigma_u^2} = \frac{2\alpha_0 - \sin 2\alpha_0}{2\alpha_0 + \sin 2\alpha_0}, \tag{28}$$

as shown in Fig. 6. For a narrow beam the above function reduces to $\frac{1}{3}\alpha_0^2$.

For two infinitely narrow cross beams intersecting at an angle $2\alpha_0$, we set

$$\mathbf{S} = F(k) \quad \text{for} \quad \alpha = -\alpha_0, \qquad \alpha = +\alpha_0,$$

and zero otherwise. This yields simply

$$\sigma_c^2/\sigma_u^2 = \tan^2 \alpha_0. \tag{29}$$

TABLE II. Beam Widths and Angular Spread Between Two Intersecting Beams, Leading to Observed Ratios of Crosswind and Up/Downwind Slope Components

	Min.	*Mean*	*Max.*	*Slick (mean)*
σ_c^2/σ_u^2	0.54	0.75	1.0	0.86
$2\alpha_0$, single beam	134°	157°	180°	167°
$2\alpha_0$, two narrow cross beams	72°	82°	90°	86°

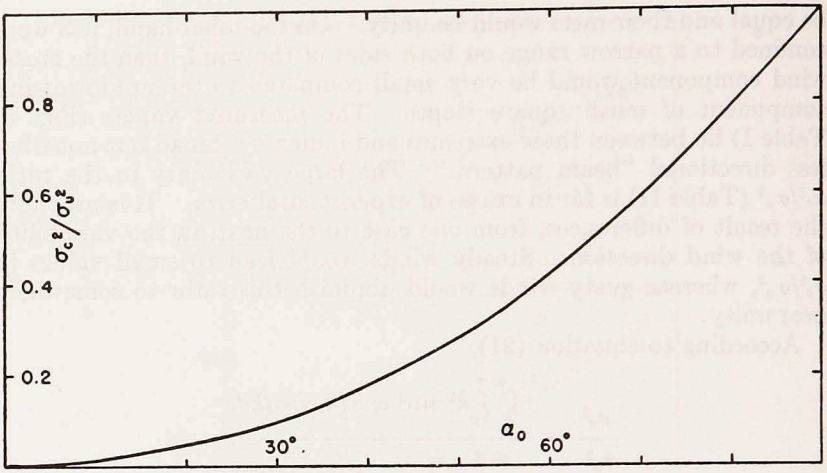

Figure 6. Half beam width of wave directions, α_0, as a function of the ratio of mean square slope components, σ_c^2/σ_u^2. It is assumed that waves of all periods have the same beam width.

The corresponding values are given in Table II. For a trade-wind sea, it is believed that the single broad beam conforms more nearly to actual conditions. The corresponding beam width is remarkably wide. For comparison, Duntley (1950) obtained $\sigma_c^2/\sigma_u^2 \simeq 0.7$ on Lake Winnipesaukee, N. H.; Schooley (1954) obtained a smaller value, about 0.4, possibly because his photographs from a bridge over the Anacostia River sampled a relatively small area with a correspondingly smaller variability in wind direction. It should be kept in mind, however, that all of these values refer to those (high frequency) components of the spectrum that contribute largely to slopes. There are no other published measurements of the directionality of ocean waves, but preliminary results obtained by Barber (personal communication) by means of an array of wave *height* recorders indicate a beam width of 90°. This agrees exactly with Arthur's (1949) estimate based on a comparison between observed and predicted waves during the invasion of Sicily. However, it is becoming clear that the beam width varies considerably with meteorological conditions, so that a great deal of further work remains to be done.

5.3 *The spectra proposed by Darbyshire and Neumann.* The period spectrum[6] $\mathbf{T}_T$ is related to the frequency spectrum $\mathbf{T}_\omega$ by the relation

[6] A choice of notation must be made between the use of frequencies and wave numbers on the one hand or of periods and wave lengths on the other hand. The physicist is more familiar with the former notation, the oceanographer with the latter.

$$\mathbf{T}_\omega |d\omega| = \mathbf{T}_T |dT|, \tag{30}$$

where $\omega = 2\pi/T$, $k = 2\pi/L$, and

$$\omega^2 = gk + \gamma k^3, \tag{31}$$

with γ designating surface tension divided by density (74 cm^3 sec^{-2} for clean water). According to (31), the phase velocity reaches a minimum value

$$C_{\min} = \omega_m/k_m = (4g\gamma)^{1/4} \tag{32}$$

when

$$\omega_m = (4g^3/\gamma)^{1/4}, \qquad k_m = (g/\gamma)^{1/2}.$$

Numerical values are $C_{\min} = 23$ cm sec^{-1}, $T_m = 0.074$ sec, $L_m = 1.7$ cm.

Waves much longer than L_m are gravity waves, and for these

$$\omega^2 \approx gk. \tag{32}$$

Waves much shorter are capillary waves, and

$$\omega^2 \approx \gamma k^3. \tag{33}$$

Darbyshire (1952) has proposed a spectrum of the variance of $z(0,t)$ equivalent to

$$\mathbf{T}_T = c'T^2 \exp\left[-2.0\left(\frac{gT}{U} - 4.6\right)^2\right], \tag{34}$$

where c' has the value 22 cm^2sec^{-3} and U is the gradient wind speed equal on the average to 1.5 times the masthead wind speed, W.

The spectrum was obtained by frequency-analysis of pressure records of waves generated by local storms at Lands End, England. Only those storm records were analyzed for which the fetch was sufficient to generate equilibrium waves. The bottom pressure transducer was usually located at a depth of 50 ft. This requires that for wave periods less than 14 sec the usual hydrodynamic relationship must be used to convert bottom pressure to surface elevation, as has been done by Darbyshire. But for periods less than 6 sec, the bottom pressure oscillations are reduced to such a low level that this is no longer

---

Most relationships are somewhat simpler in the former notation, but the integrals appearing in this section must actually be converted to the latter notation to be put into integrable form. We have made the following compromise. In sections dealing with the theory of spectra we have used the former notation. But in the following sections, where we are mostly concerned with numerical values of waves whose periods greatly exceed 1 second and whose lengths exceed 1 cm, it seemed preferable to adopt the latter convention.

practicable. Apparently these short-period waves have been ignored by Darbyshire. But it will be shown that these waves contribute about five-sixths of the total wave energy and that consequently Darbyshire's spectrum is too narrow and the total energy too small (Fig. 7). A pressure recorder at 50 ft is evidently not a suitable instrument for obtaining the energy spectrum.

On the basis of visual observations of fully developed waves in a storm area, Neumann (1953) proposed a spectrum (Fig. 5)

$$\mathbf{T}_T = \frac{1}{8} c \left(\frac{gT^2}{2\pi}\right)^2 \exp\left[-2\left(\frac{gT}{2\pi W}\right)^2\right], \tag{35}$$

where W is the wind speed and

$$c = 0.827 \times 10^{-3}\ \text{sec}^{-1}. \tag{36}$$

It is of interest to compare the Darbyshire and Neumann spectra. The periods which correspond to the maximum value of $\mathbf{T}_T$,

$$4.7\, g^{-1}U \simeq 7.1\, g^{-1}W, \qquad 2\pi g^{-1}W \tag{37}$$

respectively, are in reasonable agreement. The mean square elevations,[7] however, follow different laws:

$$6.4 \times 10^{-5}\ \text{cm}^{-1}\ \text{sec}^3\ U^3, \qquad 3.2 \times 10^{-12}\ \text{cm}^{-3}\ \text{sec}^5\ W^5. \tag{38}$$

If the observations in Darbyshire's fig. 7 are fitted to Neumann's formula and if $<z^2>$ is computed as a function of W, we find that $c = 0.3 \times 10^{-3}\ \text{sec}^{-1}$ compared to Neumann's value 0.8×10^{-3}. The small value presumably reflects the lack of information on wave periods less than $T_1 = 6$ sec. We propose to correct this value as follows. Assume Neumann's spectrum (35). The contribution of waves having periods greater than T_1 to the mean square elevation is

$$<z^2>_{T>T_1} = \int_{T_1}^{\infty} \mathbf{T}_T dT = \left(\frac{g}{2\pi}\right)^2 \frac{c}{8}\left\{\frac{1}{2} T_1^3 V^2 \left(1 + \frac{3}{2}\frac{V^2}{T_1^2}\right) e^{-T_1^2/V^2} + \frac{3}{8} V^5 \sqrt{\pi}\left[1 - H\left(\frac{T_1}{V}\right)\right]\right\}, \tag{39}$$

[7] The average kinetic and average potential energy for gravity waves equal $\frac{1}{2}\rho g <z^2>$. The potential energy due to surface tension may be estimated as follows. The increase of surface area due to waves is $\int\int_A (\sec\beta - 1)dxdy$ and the potential energy per unit area is $(g\gamma/A)\int\int(\sec\beta - 1)dxdy \simeq g\gamma\sigma^2/2$. The potential energy increases linearly with σ^2, hence it is proportional to wind speed and reaches a value of 2.8 erg cm^{-2} at $W = 14$ m sec^{-1}. According to the Neumann energy spectrum, this is 3×10^{-7} times the potential energy due to gravity waves under similar conditions.

where $V = \pi\sqrt{2}\, Wg^{-1}$ and $H(\xi) = 2\pi^{\frac{1}{2}} \int_0^{\xi} e^{-t^2}\, dt$ is the error integral.

Entering equation (39) with appropriate values of W and $<z^2>_{T>T_1}$ from Darbyshire's data and setting $T_1 = 6$ seconds, we obtain $c = 2 \times 10^{-3}$ sec^{-1} with large scatter compared to the previous value of 0.3×10^{-3} sec^{-1} (uncorrected for the high frequency cut-off) and Neumann's value 0.8×10^{-3} sec^{-1}.

5.4 *The slope spectrum and mean square slope.* The mean square slope, regardless of direction, σ^2, can be computed from $\mathbf{T}_T$ according to equations (22) and (30). *Neglecting capillary waves*, the spectra proposed by Darbyshire and Neumann yield, respectively,

$$(2\pi)^4 \sqrt{\left(\frac{1}{2}\pi\right)} (4.6)^{-2} c'(gU)^{-1} = 1.0\, W^{-1} \tag{40}$$

$$\frac{1}{2}\pi^3 \sqrt{\left(\frac{1}{2}\pi\right)} cg^{-1}W = 1.6 \times 10^{-5} W. \tag{41}$$

By the method of least squares, our observations give

$$\begin{aligned} &5.12 \times 10^{-5} W + 0.003 \pm 0.004 \\ &1.56 \times 10^{-5} W + 0.008 \pm 0.004 \end{aligned} \tag{42}$$

for the clean and slick surface, respectively. Here W is in cm sec^{-1}.

Contrary to our observations, the Darbyshire spectrum predicts that the mean square slope *decreases* with increasing wind speed. For $W = 10$ m sec^{-1}, $\sigma^2 = 10^{-3}$ compared to the observed value $(54 \pm 4) \times 10^{-3}$. Clearly the spectrum proposed by Darbyshire has too little energy in the short waves. As noted earlier, this is not surprising, since waves having periods shorter than six seconds could not have been observed.

The important result is that Neumann's spectrum yields the observed linear relation between mean square slope and wind speed.[8] Furthermore, the computed proportionality constant agrees with the measurements over slicks, but it is one third the value required to account for the clean surface. If we take the value $c = 2 \times 10^{-3}$ sec^{-1} on the basis of Darbyshire's data (corrected for high frequency cut-off), the result is

$$\sigma^2 = 4 \times 10^{-5} W.$$

[8] This fact was mentioned by W. Pierson in a paper delivered before the American Geophysical Union, May 1953.

A generalization of Neumann's spectrum of the form

$$\mathbf{T}_T \sim T^m \exp\,[-\,(T/W)^n]$$

yields

$$\sigma^2 \sim W^{m-3} \frac{1}{n} \Gamma\left(\frac{m-3}{n}\right),$$

and hence σ^2 will be proportional to W only if $m = 4$, as assumed by Neumann. Neumann states that his data are convincingly better in accord with $\mathbf{T}_T \sim T^4$ than T^3 or T^5. Of course there must be other analytic functions which also yield $\sigma^2 \sim W$. Nevertheless the consistency of Neumann's result with ours is encouraging.

Next we wish to examine whether or not an exact integration which considers capillaries leads to a measurable deviation from the linear relation between σ^2 and W. We assume without justification that Neumann's spectrum function can be extended into the high frequencies. The modification is such that for $T \ll T_m$ the slope spectrum decreases with decreasing T like $T^{8/3}$ instead of remaining constant (Fig. 7), so that the mean square slope must be less than that given by (41). It is no longer possible to obtain an integral in closed form. We derived analytic solutions for the two asymptotic cases, $W \ll c_{\min}$ and $W \gg c_{\min}$, and integrated the intermediary part by numerical methods. The resultant mean square slope is

$$\sigma^2[1 - 2.28\pi^{-\frac{1}{2}}(c_{\min}/W)] = \sigma^2 - 0.0005, \qquad (43)$$

where σ^2 is the solution (eq. 41) when capillarity is neglected. The measured intercept (eq. 42) is $+ 0.003 \pm 0.004$. The modification is evidently smaller than the uncertainty in the empirical relations.

6. THE EFFECT OF SLICKS

We wish to consider whether it is possible to account for the observed reduction by a factor of two or three of the mean square slopes. The method will in a sense be the opposite of that in Section 4.2. There we assumed a statistical balance between generation and decay. Here we propose no generation and full decay by molecular viscosity.

According to Reynolds's classical theory (Lamb, 1932: 631–632), an inextensible surface film in effect annuls the horizontal velocity at the surface. This leads to a modulus of decay of

$$\tau = 2\sqrt{2}\nu^{-\frac{1}{2}}k^{-1}\omega^{-\frac{1}{2}},$$

where ν is the kinematic viscosity. In the actual case, the film will be somewhat extensible, and the foregoing expression may be regarded as an upper limit to the effectiveness of a surface active agent. The re-

duction in (amplitude)^2 for each spectral component is exp $(-2t/\tau)$, where t is the length of time since the wave entered the slick. The time required to cross a slick of length S is $t' = Sk/\omega$, and the mean reduction (sampled by a photograph of the entire slick) is

$$F = \frac{1}{t'} \int_0^{t'} e^{-2t/\tau}\, dt = \alpha(1 - e^{-1/\alpha}),$$

where

$$\alpha = (2\omega)^{\frac{1}{2}} S^{-1} \nu^{-\frac{1}{2}} k^{-2} = 2.11 \times 10^{-4} k^{-2} \omega^{\frac{1}{2}} cgs$$

for a slick 500 m in length. For $\alpha \gg 1$, $F \approx 1$, and for $\alpha \ll 1$, $F \approx \alpha$. The two above equations with $\omega(k)$ lead to $F(T)$. This reduction factor has been applied to the (amplitude)^2 and (slope)^2 spectra, as shown in Fig. 7. For waves of 0.5 sec (1 ft length), these spectra are reduced by a factor of 100 (amplitude by a factor of 10), and thus waves shorter than this are essentially eliminated. This is in reasonable accord with visual observations. As is to be expected, the mean square amplitude is hardly affected by this "high frequency cut-off," whereas the mean square slope is appreciably reduced.

The mean square slope in the presence of slicks, $\int_0^\infty Fk^2\, \mathfrak{T}_T\, dT$, equals

$$0.34 \times 10^{-2}, \qquad 0.76 \times 10^{-2}$$

for wind speeds of 5 m sec^{-1} and 10 m sec^{-1} respectively. The corresponding ratios in mean square slope with slick as compared to those with a clean surface are

$$0.40/0.82 = 0.48, \qquad 1.13/1.65 = 0.68.$$

The observations give

$$0.55, \qquad 0.44.$$

The numerical values show rough agreement between the observed decrease in mean square slope within the slick and that computed on the basis of Reynolds' classical theory. But some serious difficulties remain. Reynolds' theory presumes a (horizontally) inextensible surface film such as one would expect to find for a monomolecular layer or for layers a few molecules thick at most. On the other hand, the thickness of the artificial slicks is estimated to be of the order of 10^{-4} cm, or 1000 molecules. This estimate follows from considerations involving the known size of the slick and of the volume of oil and from the occasional appearance of interference colors.

It is possible, however, that the oil film had an adsorbed monolayer at the air-oil or oil-water interface.[9] The compressional strength of

[9] See also Hennicker (1949). He summarizes experimental evidence for crystal-like organization of polymolecular films. Such a film would be expected to withstand static forces.

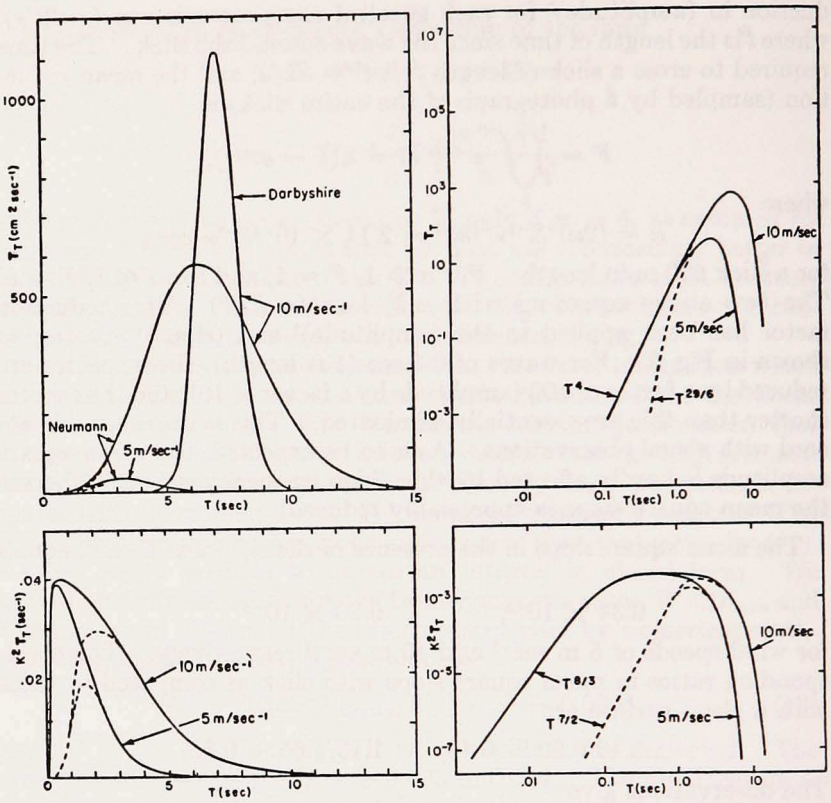

Figure 7. Period spectra of variance of sea surface elevation (upper panels) and of slope regardless of direction (lower panels). The left panels are drawn on a linear scale, the right panels on a double logarithmic scale. The asymptotic behaviour for high frequencies is indicated. Curves refer to wind speeds of 5 and 10 m sec^{-1} as noted. Solid lines apply to clean sea surface, dashed lines to slick surface. The variance of the $z(t)$ spectrum proposed by Darbyshire is illustrated on the upper left panel; all other curves are derived from Neumann's spectrum.

such a layer would be the difference between the surface tension of a clean interface ($\approx$ 40 dynes cm^{-1} for oil-water) and the surface tension of the contaminated surface ($>$ 0 dynes cm^{-1}). The following calculation shows that this would not be sufficient to annul the surface orbital velocities.

The x,y components of stress induced in the film by horizontal shear in the orbital velocity just below the film are

$$p_{xz} = \mu\left(\frac{\partial w}{\partial x} + \frac{\partial u}{\partial z}\right), \qquad p_{yz} = \mu\left(\frac{\partial w}{\partial y} + \frac{\partial v}{\partial z}\right),$$

where u,v,w are the x,y,z components of orbital velocity of the waves, μ is the viscosity, and the derivatives are to be evaluated at the surface. Let $\mathbf{p}$ be the vector shear whose components are p_{xz} and p_{yz}. For an infinitesimal wave train in the direction $\mathbf{k}$ (unit vector $\mathbf{k}_1$) of elevation

$$Re\ \{A \exp\ [i(kr - \omega t)]\} kdkd\alpha,$$

the appropriate formula is (Lamb: Arts. 349, 351)

$$\mathbf{p} = \mathbf{k}_1 \omega^{3/2} (\rho\mu)^{\frac{1}{2}}\ Re\ \left\{A \exp\left[i\left(\mathbf{k}\cdot\mathbf{r} - \omega t - \frac{\pi}{4}\right)\right]\right\} kdkd\alpha.$$

Consider two points, $\mathbf{r}_1$ and $\mathbf{r}_2$, and let $\Delta\mathbf{r} = \mathbf{r}_2 - \mathbf{r}_1$. Then, if there is no shear strength in the film, the scalar

$$F_{12} = \int_{\mathbf{r}_1}^{\mathbf{r}_1} \mathbf{p}\cdot d\mathbf{r}$$

is the *difference* in tension between the two points. For the wave train, this gives

$$F_{12} = 2\omega^{3/2} (\rho\mu)^{\frac{1}{2}} k^{-1} \sin\ (\tfrac{1}{2}\mathbf{k}\cdot\Delta\mathbf{r})\ \ Re\left\{A \exp i\left(\mathbf{k}\cdot\mathbf{r} - \omega t - \frac{\pi}{4}\right)\right\} kdkd\alpha.$$

For a continuous spectrum of waves, the mean square tension can be shown to equal

$$<F_{12}^2> = 4\rho\mu \iint \omega^3 k^{-2} \sin^2 (\tfrac{1}{2}\mathbf{k}\cdot\Delta\mathbf{r})\mathbf{S}kdkd\alpha.$$

For sufficiently large values of Δr, the $(\sin)^2$ factor, which oscillates rapidly, may be replaced by its average value, $\frac{1}{2}$, and the integration over α may be performed:

$$<F_\infty^2> = 2\rho\mu \int_0^\infty \omega^3 k^{-2}\, \mathbf{T}_T dT.$$

Assuming the Neumann spectrum for $\mathbf{T}_T$, and setting $\omega^3 k^{-2} = g^2 T/2\pi$, (gravity waves) yields

$$<F_\infty^2> = \rho\mu \frac{(2\pi)^3 c W^6}{32\, g^2} = 6 \times 10^7 \left(\frac{W}{10 \text{ m sec}^{-1}}\right)^6 (\text{dyne cm}^{-1})^2.$$

The required strength is therefore far in excess of 40 dynes/cm. But the large value reflects primarily the stresses due to the long period waves. To estimate the longest waves which will not readily rupture the film, we may set

$$2\rho\mu \int_0^{T_{max}} \omega^3 k^{-2} \mathbf{T}_T dT = (40 \text{ dyne cm}^{-1})^2.$$

Neglecting capillary waves, this gives

$$T_{max} = (24)^{1/6}(2\pi)^{\frac{1}{2}}(\rho g^4 \mu c)^{-1/6}(40 \text{ dyne cm}^{-1})^{1/3} = 0.7 \text{ sec.}$$

The principal reduction in σ^2 by slicks has been attributed to waves of period greater than 0.7 sec (Fig. 7).

No allowance for generation and decay (other than by molecular processes) has been made in the present calculation. An alternate hypothesis for the effectiveness of slicks is that they damp only high frequency wave components and that, in absence of these components, the balance between generation and decay is thrown in favor of decay for low-frequency components. This matter needs further investigation.

7. THE SPECTRUM OF ACCELERATION

The horizontal acceleration of an elementary wave train, $A \cos (kx - \omega t)$, has an amplitude $\omega^2 A$ at the sea surface. For gravity waves this equals gkA. The slope has an amplitude kA. Except for a minor contribution from capillaries (see end of Section 5.4), *the distribution of acceleration (in units of g) and of slope (in radians) are equivalent:*[10]

$$a_c^2 = \sigma_c^2, \qquad a_u^2 = \sigma_u^2,$$

where a_c^2 and a_u^2 are the crosswind and up/downwind components of the mean square acceleration (in units of g) at the sea surface. The mean square horizontal acceleration, regardless of direction, is therefore

$$a_h^2 = a_c^2 + a_u^2 = \sigma^2.$$

The mean square vertical acceleration a_v^2 for deep water waves equals the horizontal acceleration, and the mean square acceleration in all three directions is

$$a^2 = a_h^2 + a_v^2 = 2\sigma^2.$$

Preceding results regarding the slope distribution can be applied directly. Thus the up/downwind component exceeds the crosswind component of mean square acceleration by a factor of 1.3, on the average; all mean square accelerations increase linearly with wind, and the total rms acceleration at a wind speed of 14 m sec^{-1} is 0.4 g!

The horizontal acceleration spectrum is $\omega^4 \mathbf{T}_T$, and the mean square acceleration,

$$a_h^2 = \int_0^\infty \omega^4 \mathbf{T}_T dT = \pi^3 \sqrt{\left(\frac{\pi}{2}\right)} \frac{cW}{2g},$$

varies *exactly* in proportion to wind speed according to the Neumann spectrum.

[10] This was first pointed out to us by N. F. Barber (personal communication).

REFERENCES

ARTHUR, R. S.

1949. Variability in the direction of wave travel. Ann. N. Y. Acad. Sci., *51:* 511–522.

CHANDRASEKHAR, S.

1943. Stochastic problems in physics and astronomy. Rev. mod. Phys., *15:* 1–89.

COX, CHARLES AND W. H. MUNK

1953. Air Force Technical Reports No. 2, 3, 4, SIO Ref. 52–61, 53–53, 54–10 (unpub).

1954. The measurement of the roughness of the sea surface from photographs of the sun's glitter. J. opt. Soc. Amer. (In press)

DARBYSHIRE, J.

1952. The generation of waves by wind. Proc. Roy. Soc. (A) *215:* 299–328.

DUNTLEY, S. Q.

1950. The visibility of submerged objects: Part I. Optical effects of water waves. Rep. Visibility Lab., Mass. Inst. Techn., Dec. 15, 1950; U. S. Off. Naval Res. Rep. No. N5 ori-07831.

ECKART, CARL

1953. The scattering of sound from the sea surface. J. acoust. Soc. Amer., *25:* 566–570.

HENNICKER, J. C.

1949. The depth of the surface zone of a liquid. Rev. mod. Phys., *21:* 322–341.

LAMB, H.

1932. Hydrodynamics. Cambridge University Press, London. 738 pp.

LONGUET-HIGGINS, M. S.

1950. A theory of the origin of microseisms. Phil. Trans., *243:* 1–35.

NEUMANN, G.

1953. On ocean wave spectra and a new method of forecasting wind generated sea. Technical Memoirs, Beach Erosion Board.

PIERSON, W. J. AND W. MARKS

1952. The power spectrum analysis of ocean wave records. Trans. Amer. geophys. Un., *33:* 834–844.

RICE, S. O.

1944. Mathematical analysis of random noise. Bell Syst. tech. J., *23:* 282–332.

SCHOOLEY, A. H.

1954. A simple optical method for measuring the statistical distribution of water surface slopes. J. opt. Soc. Amer., *44:* 37–40.

SYŌNO, S.

1953. Frequency distribution functions of velocities in turbulent flow. J. met. Soc. Japan, *31:* 299–305.

TITCHMARSH, E. C.

1937. Introduction to the theory of Fourier integrals. Oxford Clarendon Press, London. 390 pp.

WIENER, N.

1933. The Fourier integral and certain of its applications. Cambridge University Press, London. 201 pp.